

# Relaxation Behavior Study of Ultrasmall Superparamagnetic Iron Oxide Nanoparticles at Ultralow and Ultrahigh Magnetic Fields

Wei Wang,<sup>\*,†,‡</sup> Hui Dong,<sup>‡,§</sup> Victor Pacheco,<sup>||,⊥,‡</sup> Dieter Willbold,<sup>||,‡</sup> Yi Zhang,<sup>‡</sup> Andreas Offenhaeusser,<sup>‡</sup> Rudolf Hartmann,<sup>||</sup> Thomas E. Weirich,<sup>▽</sup> Peixiang Ma,<sup>||</sup> Hans-Joachim Krause,<sup>‡</sup> and Zhongwei Gu<sup>\*,†</sup>

<sup>†</sup>National Engineering Research Center for Biomaterials, Sichuan University, 610064 Chengdu, China

<sup>‡</sup>Peter Gruenberg Institute (PGI-8), Research Center Juelich, 52425 Juelich, Germany

<sup>§</sup>State key Laboratory of Functional Materials for Informatics, Shanghai Institute of Microsystem and Information Technology, Chinese Academy of Sciences, 200050 Shanghai, China

<sup>||</sup>Institute of Complex Systems (ICS-6), Research Center Juelich, 52425 Juelich, Germany

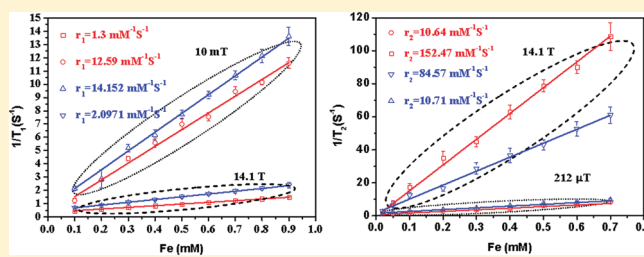
<sup>⊥</sup>Central Division of Analytical Chemistry (ZCH), Research Center Juelich, 52425 Juelich, Germany

<sup>#</sup>Institut für Physikalische Biologie, Heinrich-Heine-Universität Düsseldorf, 40225 Düsseldorf, Germany

<sup>▽</sup>Central Facility for Electron Microscopy and Institute of Crystallography, RWTH Aachen University, 52074 Aachen, Germany

 Supporting Information

**ABSTRACT:** Ultrasmall superparamagnetic iron oxide nanoparticles (USPIOs) have attracted attention because of their current and potential usefulness as contrast agents for magnetic resonance imaging (MRI) and nuclear magnetic resonance (NMR). USPIOs are usually used for their significant capacity to produce predominant proton relaxation effects, which result in signal reduction. However, most previous studies that utilized USPIOs have been focused on the relaxation behavior at commonly used magnetic fields of clinical MRI systems (typically 1–3 T). In this paper, magnetic relaxation processes of protons in water surrounding the USPIOs are studied at ultralow ( $\leq 10$  mT) and ultrahigh magnetic fields (14.1 T). USPIOs used in our experiments were synthesized with a core size of 6 nm, and transferred from organic to water by ligand exchange. The proton spin–lattice relaxation time ( $T_1$ ) and spin–spin relaxation time ( $T_2$ ) were investigated at ultralow (212  $\mu$ T for  $T_2$  and 10 mT for  $T_1$ ) and at 14.1 T with different iron concentrations. At all of the fields, there is a linear relationship between the inverse of relaxation times and the iron concentration. The spin–spin relaxivity ( $r_2$ ) at 14.1 T is much larger than that value of the ultralow field. At ultralow field, however, the spin–lattice relaxivity ( $r_1$ ) is larger than the  $r_1$  at ultrahigh field. The results provide a perspective on potential in vivo and in vitro applications of USPIOs in ultralow and ultrahigh field NMR and MRI.



## 1. INTRODUCTION

Ultrasmall superparamagnetic iron oxide nanoparticles (USPIOs) with diameters of less than 40 nm,<sup>1</sup> have been widely studied in in vivo and in vitro applications, such as magnetic resonance imaging (MRI),<sup>2</sup> drug delivery,<sup>3</sup> biomagnetic separation,<sup>4</sup> and biosensing applications,<sup>5,6</sup> because of their property to shorten the proton relaxation time of surrounding water. Compared with larger superparamagnetic iron oxide nanoparticles (SPIOs), which are usually utilized as  $T_2$ -weighted contrast agents, USPIOs exhibit a lower proton spin–spin relaxivity ( $r_2 = 1/T_2$ , where  $T_2$  is the proton spin–spin relaxation time) at clinical fields (1–3 T).<sup>7</sup> Normally, they are also suited for MR angiography as  $T_1$ -weighted contrast agents.<sup>8,9</sup>

In clinical fields, the relaxation behavior of SPIOs and USPIOs has been well studied and discussed.<sup>10,11</sup> Bulte et al.<sup>12</sup> showed and explained the  $r_1$  and  $r_2$  field dependence of SPIOs suspensions. In further studies, the “three-phase model” theory<sup>10</sup> was

reported for USPIO suspensions, which leads to an increase of the magnetization at high fields and also causes the enhancement of  $r_2$  at high fields. Moreover, Corot et al.<sup>7</sup> investigated the influence of USPIO aggregation on relaxation properties, reporting that  $r_1$  would slightly decrease with increasing aggregation, whereas  $r_2$  would increase considerably.

However, the investigation of USPIOs relaxation behavior at ultralow or ultrahigh fields has been rarely done. With the development of ultralow field MRI systems (from 1  $\mu$ T to 10 mT) based on superconducting quantum interference devices (SQUIDs) as magnetic field detector,<sup>13</sup> applications of USPIOs at these extremely low fields become feasible. On the other hand, ultrahigh field systems based on MRI (3 T and more, now even

Received: July 12, 2011

Revised: September 30, 2011

Published: October 05, 2011

11.7 T) and nuclear magnetic resonance (NMR) instruments (7 to 23.5 T) have been developed in recent years.

In this paper, the relaxation behavior of USPIOS with 6 nm diameter are investigated at ultralow field (212  $\mu$ T for  $T_2$  measurements and 10 mT for proton spin–lattice relaxation time  $T_1$  measurements) and at ultrahigh field (14.1 T). The relaxation times  $T_1$  and  $T_2$  were measured with iron concentrations ranging from 0.02 mM and 0.5 mM, and the corresponding relaxivities  $r_1$  and  $r_2$  were calculated.

## 2. EXPERIMENTAL METHODS

**2.1. Synthesis of Magnetic Nanoparticles.** USPIOS were synthesized by the thermal decomposition method.<sup>14</sup> In a typical experiment, Fe(acac)<sub>3</sub> (2 mmol), 1,2-hexadecanediol (10 mmol), oleic acid (6 mmol), oleylamine (6 mmol), and benzyl ether (20 mL) were mixed and magnetically stirred under argon. The mixture was heated to 200 °C with a constant heating rate of 3.3 °C min<sup>-1</sup> and kept at that temperature for 2 h. Then the mixture was heated to reflux (300 °C) for 1 h. After the mixture cooled to room temperature, excessive ethanol was added, and the solution was centrifuged at 4000 rpm for 10 min. The obtained precipitate were dispersed in 10 mL hexane and centrifuged at 8000 rpm. Finally USPIOS with 6 nm diameter and a narrow size distribution were obtained.

**2.2. Surface Modification.** The hydrophobic coating oleic acid on the surface of USPIO was replaced by a hydrophilic 2,3-dimercaptosuccinic acid (DMSA) or *n*-(trimethoxysilylpropyl)-ethylene diamine triacetic acid (45% in water) (carboxylic acid-silane) layer, following a previously reported protocol.<sup>2,15,16</sup>

To form the DMSA layer, 30 mg of USPIOS was dissolved in 3 mL of toluene. Subsequently, a solution of 90 mg of DMSA in 3 mL of dimethyl sulfoxide (DMSO) was added to the mixture, and stirred for 24 h. After that, excessive toluene was added to the mixture reaction, and the precipitation was isolated by magnetic separation. The precipitated nanoparticles were successively mixed and magnetic separated with acetone and hexane several times to remove free oleic acid molecules. The resulting USPIOS were redispersed in 3 mL Milli-Q water. After aggregated USPIOS were removed by passing the solution through a 0.2  $\mu$ m syringe filter, monodisperse USPIOS were obtained.

Similar to the formation of the DMSA coating, the carboxylic acid-silane layer of USPIOS was obtained after ligand exchange of oleic acid with carboxylic acid-silane. In the protocol, carboxylic acid-silane solution was added to a dispersion of oleic acid coating USPIOS in hexane containing acetic acid. After being shaken for 72 h, the precipitate was separated using a magnet. After purification by hexane/pentane to remove excess silane, it was finally redispersed in deionized water.

**2.3. Relaxivity Measurements.** NMR relaxation times ( $T_1$ , spin–lattice relaxation, and  $T_2$ , spin–spin relaxation) are indicative for various intra- and intermolecular spin couplings.<sup>17</sup> The iron concentration of the USPIOS samples was measured by a inductively coupled plasma optical emission spectrometer (ICP-OES), and adjusted to values between 0.02 and 0.5 mmol/L.

**2.3.1. Ultralow Field NMR Measurement with SQUID.** Low-field relaxation measurements of the samples were performed at 10 mT for  $T_1$  measurement and at 212  $\mu$ T for  $T_2$  measurement with our homemade ultralow-field NMR system. This system utilized a tuned high- $T_c$  (HTS) SQUID as a detector, consisting of a radio frequency (rf) SQUID magnetometer and a liquid-nitrogen-cooled (LC) resonant circuit, which were inductively

coupled. The SQUID was fabricated by laser ablation of yttrium–barium–copper-oxide thin films on a lanthan aluminate single crystal substrate with a ditch etched into it to form a single step-edge Josephson junction. The SQUID is read out inductively with a strontium titanate single crystal substrate resonator equipped with a flux focuser structure using our rf readout electronics. Our experiments were performed in a magnetically shielded room. The sample of 20 mL was filled in a glass vial and placed directly below the liquid nitrogen dewar for sensor cooling, thus being located about 20 mm away from the magnetometer. The measurement field  $B_m$  was 212  $\mu$ T, corresponding to the Larmor frequency of 9 kHz. The resonant frequency of tuned SQUID was adjusted to be around 9 kHz, at which frequency the sensitivity of the system reached 6–7 fT/√Hz.

In the low field NMR measurements, the sample was repeatedly magnetized in the prepolarization field generated by a solenoid around the vial for a time  $t_{BP}$  of typically 5 s with a magnitude of 10 mT. Polarizing field, measurement field, and sensitive direction of the SQUID magnetometer form an orthogonal tripel. The free induction decay (FID) was then measured after sudden quick shut-off of the polarization field. The system is equipped with a Q-spoiler circuit at the resonant SQUID detector, which prevents ringing upon polarization field shut-off. The spin echo chain was recorded after the application of a series of  $\pi$  pulse at 9 kHz. The system setup and pulse sequence were described in detailed in ref 18. The measurement of  $T_1$  relaxation time was realized by increasing the duration  $t_{BP}$  step by step until the saturation of sample magnetization and fitting of the spectral amplitudes  $A_1(t_{BP})$  with  $A_1(t_{BP}) = A_1[1 - \exp(-t_{BP}/T_1)]$ . For the measurement of  $T_2$  relaxation time, the Carr–Purcell–Meiboom–Gill (CPMG) pulse sequence<sup>19,20</sup> consisting of a series of  $\pi$  pulses was applied after the FID signal to subsequently recover spin echoes. To each spin echo maximal amplitude  $A_2(t)$  at time  $t$ , an envelope function  $A_2(t) = A_2 \cdot \exp(t/T_2)$  with the time constant  $T_2$  was then fitted.

**2.3.2. Ultrahigh Field NMR Measurement.** The ultrahigh field proton relaxation times  $T_1$  and  $T_2$  were measured on a 600 MHz Varian INOVA spectrometer. The measurements were determined by applying the inversion–recovery pulse sequence and the CPMG pulse sequence without spinning.

All samples were measured at 25 ± 0.1 °C after 10 min of temperature equilibration within the magnet. Shimming for all samples was checked and adjusted individually by gradient shimming and by hand (the line width was minimized to be less than 3 Hz).<sup>21</sup> For each sample, 8  $\mu$ L capillaries were measured individually and placed in a standard 5-mm NMR tube with centering. Each experiment was repeated five times and then averaged.

We measured the dependence of  $T_1$  and  $T_2$  based on the different iron concentration of USPIOS. For all the investigated solution, the magnetization decays could be nicely fitted by the monoexponent function of relaxation times.  $T_1$  was between 0.74 and 3.20 s,  $T_2$  between 0.01 and 2.97 s. In all data sets, a single capillary of deionized water was measured several times as the control sample.

## ■ RESULTS AND DISCUSSION

Monodisperse USPIOS were synthesized with surfactant at high temperature. Figure 1A,B depicts the transmission electron microscopy (TEM) and scanning transmission electron

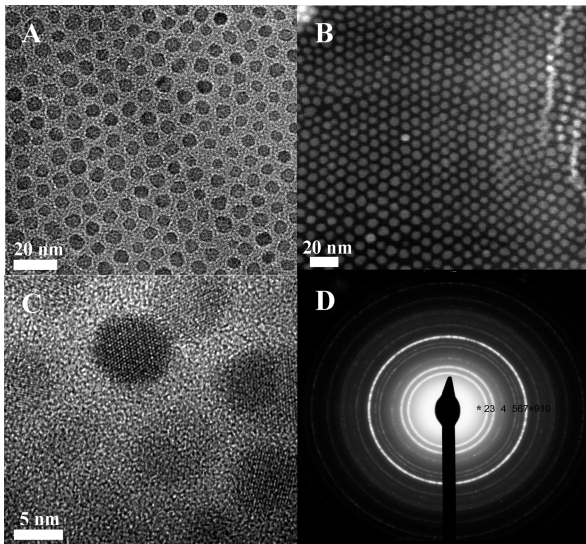


**Figure 1.** TEM bright field images of USPIOs (A); STEM of USPIOs (B); HRTEM image of a single 6 nm USPIO (C); and SAED pattern acquire from a 6 nm USPIO assembly (D).

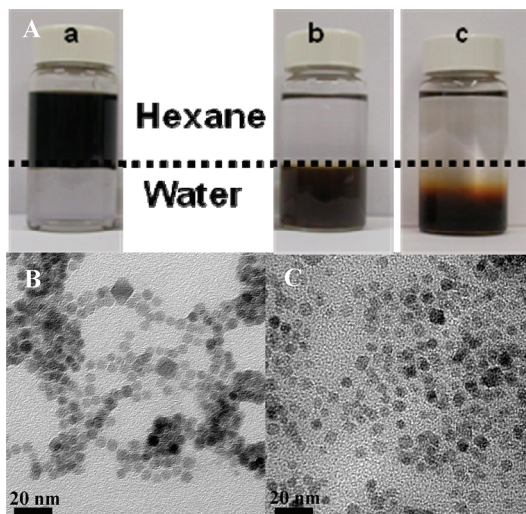


**Figure 2.** Solubility test (A) of USPIOs dispersed in hexane (bottle a) and dispersed in water after DMSA ligand exchange (bottle b) and carboxylic acid-silane ligand exchange (bottle c), respectively; TEM images of DMSA-coated (B), and carboxylic acid-silane-coated (C) USPIOS.

microscopy (STEM) images of 6 nm USPIOS. Obtained USPIOS are highly single-phased crystalline with a narrow size distribution. Figure 1C shows the high-resolution TEM (HRTEM) image of a single USPIO. The measured distance between adjacent planes is 3.03 Å, which corresponds to  $\text{Fe}_3\text{O}_4$  (220) planes. The selected area electron diffraction (SAED) pattern acquired from the USPIO is shown in Figure 1D.

USPIOS that are coated with hydrophobic surfactants are insoluble in water (see bottle a of Figure 2A). A simple but highly effective method to disperse USPIOS in water is introduced by replacing the hydrophobic surface with hydrophilic molecules ligands. The DMSA binds to the USPIO surface through its carboxylic bonding, and the intermolecular disulfide cross-linking between surface-bound DMSA ligands strengthens the

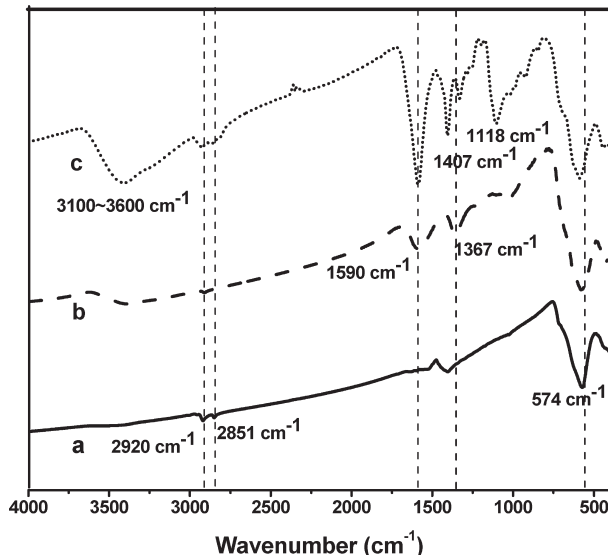


**Figure 3.** Transmission IR spectra for USPIOs before (a) and after DMSA (b) and carboxylic acid-silane (c) ligand exchange processes.

nanocrystal stability. The carboxylic acid-silane also forms a stable polymer coating up to three binding sites per Si atom to the iron oxide.<sup>16</sup> In TEM images of DMSA and carboxylic acid-silane coated USPIOS, presented in Figure 2B,C, the USPIOS retain their original size of 6 nm without aggregation. Since our water-soluble iron oxide USPIOS present high monodispersity and stability in aqueous media with enhanced magnetic properties, the USPIOS were well dispersed in water (see bottles b and c of Figure 2A). In our experiment, there was no precipitation of USPIOS within 6 weeks. The particles remained stable in phosphate buffered saline (PBS) for at least 8 h at pH 7.4 (see Supporting Information).

Representative IR spectra are shown in Figure 3. The data measured before (curve a) and after (curves b and c) ligand exchange indicate that DMSA and carboxylic acid-silane are bound to the surface of the USPIOS. In Figure 3b, the appearance of a broad asymmetric peak from  $1500 \text{ cm}^{-1}$  to  $1700 \text{ cm}^{-1}$  is attributed to the  $\text{C}=\text{O}$  bond of DMSA molecules, thus confirming the DMSA coating on the surface of the USPIO after ligand exchange process. Because of the formation of the  $-\text{S}-\text{S}-$  groups on the surface of the nanoparticles, the broad peak between  $600 \text{ cm}^{-1}$  and  $500 \text{ cm}^{-1}$  was increased (see Figure 3b). A broadening of the  $\text{Fe}-\text{O}$  band at  $580 \text{ cm}^{-1}$  was observed in Figure 3c, which is attributed to the formation of the  $\text{Fe}-\text{O}-\text{Si}$  bonds in silica layer. The vibrations at  $1590 \text{ cm}^{-1}$  and  $1407 \text{ cm}^{-1}$  were caused by the  $\text{COO}^-$  stretching of carboxylic acid-silane on the surface. The appearance of  $\text{Si}-\text{O}-\text{Si}$  vibrations at  $1118 \text{ cm}^{-1}$  indicates the successful modification of carboxylic acid-silane on the nanoparticle surface.

To study the relaxation behavior, we measured the  $T_1$  and  $T_2$  relaxation times of protons in water solution of USPIOS-DMSA and USPIOS-carboxylic acid-silane at low fields of 10 mT and  $212 \mu\text{T}$ , respectively. According to these relaxation measurements,  $r_1$  and  $r_2$  were calculated from the linear relationship between the inverse of relaxation times and the iron concentration. Figure 4A,C shows the relaxation curve for  $r_1$  against iron concentration of USPIOS-DMSA and USPIOS-carboxylic acid-silane, respectively. For the proton spin-lattice relaxivity, the value of  $r_1$  for USPIOS-DMSA is  $12.59 \text{ mM}^{-1} \text{ s}^{-1}$  at 10 mT,

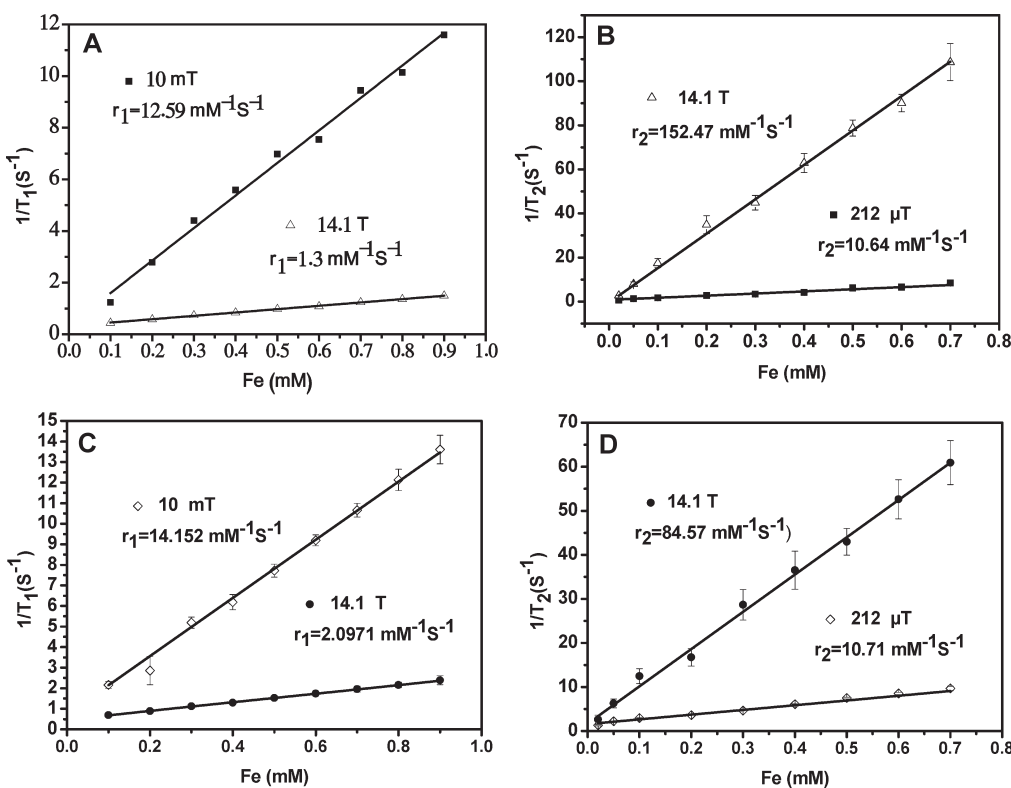


**Figure 4.** Longitudinal relaxation rate ( $1/T_1$ ) and transverse relaxation rate ( $1/T_2$ ) for USPIOS-DMSA (A,B) and USPIOS-carboxylic acid-silane (C,D), respectively, against iron concentration at 212  $\mu\text{T}$ , 10 mT, and 14.1 T.

which is larger than that of ultrahigh field ( $1.3 \text{ mM}^{-1}\text{s}^{-1}$  at 14.1 T). For USPIOS-carboxylic acid-silane, the  $r_1$  at 10 mT ( $14.152 \text{ mM}^{-1}\text{s}^{-1}$ ) is also much greater than the  $r_1$  at 14.1 T ( $2.0971 \text{ mM}^{-1}\text{s}^{-1}$ ). It is corresponding to the proton relaxation model of USPIOS, in which model the value of  $r_1$  would be stable at low field (less than 0.02 T), while at high-field the  $r_1$  would be decreased to zero.<sup>22</sup>

It is noted that the value of  $r_2$  is  $10.64 \text{ mM}^{-1}\text{s}^{-1}$  at 212  $\mu\text{T}$  for USPIOS-DMSA (Figure 4, B), which is similar with the  $10.71 \text{ mM}^{-1}\text{s}^{-1}$  of  $r_2$  for USPIOS-carboxylic acid-silane (Figure 4C). It could be explained by the similar magnetization of these two kinds of water-dispersed USPIOS at the ultralow field. Moreover, in the light of the relaxation model,<sup>10</sup> the  $r_1$  value at 212  $\mu\text{T}$  would be the same as that at 10 mT, indicating that the  $r_2/r_1$  ratio is 0.845 for USPIOS-DMSA and 0.757 for USPIOS-carboxylic acid-silane at 212  $\mu\text{T}$ . Both of these values are much lower than the ratio of commercial USPIOS such as NC100150 (1.65 at 0.47 T)<sup>23</sup> and AMI-227 (1.88 at 0.47 T and 4.49 at 1.5 T),<sup>12</sup> which have been well applied for macrophage imaging,<sup>24</sup> blood pool imaging,<sup>25</sup> and brain tumor detection<sup>26</sup> as a  $T_1$ -weighted contrast agent at clinical field. This presents the excellent potential effectiveness of the USPIOS as  $T_1$ -weighted contrast agents at an ultralow field system.

It is believed that USPIOS exhibit higher  $r_2$  with increasing magnetic field; meanwhile the  $r_1$  should decrease, leading to a rise of the ratio of  $r_2/r_1$ . In our experiment, we enhanced measurement field to 14.1 T, calculating the value of  $r_2$  as  $152.47 \text{ mM}^{-1}\text{s}^{-1}$  for USPIOS-DMSA and the  $r_2/r_1$  ratio increased to 117.29. That value is higher than the published results with similar DMSA coating magnetic nanoparticles at 1.5 T ( $101 \text{ mM}^{-1}\text{s}^{-1}$ ),<sup>27,28</sup> and even higher than literature values at 9.4 T (9 nm,  $116 \text{ mM}^{-1}\text{s}^{-1}$ ).<sup>29</sup>

It could be explained by the “three-phase model” theory, which illustrates the rise of  $r_2$  even beyond saturation of the USPIO magnetization.

Because of the shielding of the magnetization by the silica layer on the USPIOS, the  $r_2$  of USPIOS-carboxylic acid-silane is lower ( $84.57 \text{ mM}^{-1}\text{s}^{-1}$ ), leading to a  $r_2/r_1$  ratio of 40.33. However, these values are still much higher than the  $r_2/r_1$  value of 1.97 for USPIOS MION-46 L at 0.47 T and 4.96 at 1.5 T.<sup>30</sup> It is concluded that with increasing measurement field, the  $T_2$ -weighted effectiveness of USPIOS enhances remarkably, indicating that the USPIOS would be more suitable to be used as  $T_2$ -weighted contrast agents at high field.

## CONCLUSION

We have prepared high-quality USPIOS and performed ligand exchange to disperse them in water, and two kinds of water dispersed USPIOS were obtained. Both of these two kinds of USPIOS influence water proton relaxation. In our experiment, for USPIOS-DMSA, the ratio of  $r_2/r_1$  is 117.29, which can provide excellent signals at 14.1 T. Thus, when the measurement field is high enough, USPIOS can be used as the  $T_2$ -weighted agents. However, the ratio of  $r_2/r_1$  is only 0.845 and 0.757 at 212  $\mu\text{T}$  for USPIOS-DMSA and USPIOS-carboxylic acid-silane, respectively. It is illustrated that for USPIOS, a higher  $r_1/r_2$  ratio could be obtained at ultralow fields, thus indicating that the USPIOS are more suitable as  $T_1$ -weighted contrast agents in that case. We believe the results provide new perspectives on potential in vivo and in vitro applications of USPIOS as contrast agents or magnetic sensors in ultralow and ultrahigh field NMR and MRI.

## ■ ASSOCIATED CONTENT

**S Supporting Information.** Measured lattice spacing  $d$  ( $\text{\AA}$ ) based on the rings in the SAED pattern; schematic of the replacement of oleic acid coating on the surface of the USPIOs by a hydrophilic DMSA-layer; and DMSA-coated USPIOs in PBS after 8 and 10 h, and solubility test of USPIOs in water with DMSA and carboxylic acid-silane coating after 6 weeks. This material is available free of charge via the Internet at <http://pubs.acs.org>.

## ■ AUTHOR INFORMATION

### Corresponding Author

\*E-mail: zwgu@scu.edu.cn (Z.G); w.wang@fz-juelich.de (W.W.).

## ■ ACKNOWLEDGMENT

We would like to thank F. Dorn for TEM imaging, J. Bachhausen for IR measurements, and H. Lippert for the ICP-OES measurements. This work is supported by the Research Center Juelich, the China Scholarship Council (CSC), and the German Helmholtz Association.

## ■ REFERENCES

- (1) Mornet, S.; Vasseur, S.; Grasset, F.; Duguet, E. *J. Mater. Chem.* **2004**, *14*, 2161.
- (2) Huh, Y. M.; Jun, Y. W.; Song, H. T.; Kim, S.; Choi, J. S.; Lee, J. H.; Yoon, S.; Kim, K. S.; Shin, J. S.; Suh, J. S.; Cheon, J. *J. Am. Chem. Soc.* **2005**, *127*, 12387.
- (3) Vonarbourg, A.; Passirani, C.; Saulnier, P.; Benoit, J. P. *Biomaterials* **2006**, *27*, 4356.
- (4) Shukoor, M. I.; Natalio, F.; Tahir, M. N.; Divekar, M.; Metz, N.; Therese, H. A.; Theato, P.; Ksenofontov, V.; Schroder, H. C.; Muller, W. E. G.; Tremel, W. *J. Magn. Magn. Mater.* **2008**, *320*, 2339.
- (5) Lee, H.; Sun, E.; Ham, D.; Weissleder, R. *Nat. Med.* **2008**, *14*, 869.
- (6) Koh, I.; Hong, R.; Weissleder, R.; Josephson, L. *Angew. Chem., Int. Ed.* **2008**, *47*, 4119.
- (7) Corot, C.; Robert, P.; Idee, J. M.; Port, M. *Adv. Drug Delivery Rev.* **2006**, *58*, 1471.
- (8) Persigehl, T.; Bieker, R.; Matuszewski, L.; Wall, A.; Kessler, T.; Kooijman, H.; Meier, N.; Ebert, W.; Berdel, W. E.; Heindel, W.; Mesters, R. M.; Bremer, C. *Radiology* **2007**, *244*, 449.
- (9) Trattnig, S.; Pinker, K.; Ba-Ssalamah, A.; Nobauer-Huhmann, I. M. *Eur. Radiol.* **2006**, *16*, 1280.
- (10) Bulte, J. W. M.; Brooks, R. A.; Moskowitz, B. M.; Bryant, L. H.; Frank, J. A. *Magn. Reson. Med.* **1999**, *42*, 379.
- (11) Gillis, P.; Koenig, S. H. *Magn. Reson. Med.* **1987**, *5*, 323.
- (12) Bulte, J. W. M.; Vymazal, J.; Brooks, R. A.; Pierpaoli, C.; Frank, J. A. *JMRI: J. Magn. Reson. Imaging* **1993**, *3*, 641.
- (13) Clarke, J.; Hatridge, M.; Mossle, M. *Annu. Rev. Biomed. Eng.* **2007**, *9*, 389.
- (14) Sun, S. H.; Zeng, H.; Robinson, D. B.; Raoux, S.; Rice, P. M.; Wang, S. X.; Li, G. X. *J. Am. Chem. Soc.* **2004**, *126*, 273.
- (15) Jun, Y. W.; Huh, Y. M.; Choi, J. S.; Lee, J. H.; Song, H. T.; Kim, S.; Yoon, S.; Kim, K. S.; Shin, J. S.; Suh, J. S.; Cheon, J. *J. Am. Chem. Soc.* **2005**, *127*, 5732.
- (16) De Palma, R.; Peeters, S.; Van Bael, M. J.; Van den Rul, H.; Bonroy, K.; Laureyn, W.; Mullens, J.; Borghs, G.; Maes, G. *Chem. Mater.* **2007**, *19*, 1821.
- (17) Bloembergen, N.; Purcell, E. M.; Pound, R. V. *Phys. Rev.* **1948**, *73*, 679.
- (18) Dong, H.; Zhang, Y.; Krause, H. J.; Xie, X. M.; Braginski, A. I.; Offenhausser, A. *Supercond. Sci. Technol.* **2009**, *22*.
- (19) Meiboom, S.; Gill, D. *Rev. Sci. Instrum.* **1958**, *29*, 688.
- (20) Carr, H. Y.; Purcell, E. M. *Phys. Rev.* **1954**, *94*, 630.
- (21) Baumgartner, S.; Wolf, M.; Skrabal, P.; Bangerter, F.; Heusser, P.; Thurneysen, A.; Wolf, U. *Naturwissenschaften* **2009**, *96*, 1079.
- (22) Laurent, S.; Forge, D.; Port, M.; Roch, A.; Robic, C.; Elst, L. V.; Muller, R. N. *Chem. Rev.* **2008**, *108*, 2064.
- (23) Bjornerud, A.; Wendland, M. F.; Johansson, L.; Ahlstrom, H. K.; Higgins, C. B.; Oksendal, A. *Academic Radiology* **1998**, *5*, S223.
- (24) Schroeter, M.; Saleh, A.; Wiedermann, D.; Hoehn, M.; Jander, S. *Magn. Reson. Med.* **2004**, *52*, 403.
- (25) Corot, C.; Violas, X.; Robert, P.; Gagneur, G.; Port, M. *Invest. Radiol.* **2003**, *38*, 311.
- (26) Neuwelt, E. A.; Manninger, S. P.; Muldoon, L. L.; Nesbit, G.; Murillo, T.; Jacobs, P. M. *Am. J. Neuroradiol.* **2005**, *26*, 2290.
- (27) Suh, J. S.; Lee, J. H.; Huh, Y. M.; Jun, Y.; Seo, J.; Jang, J.; Song, H. T.; Kim, S.; Cho, E. J.; Yoon, H. G.; Cheon, J. *Nat. Med.* **2007**, *13*, 95.
- (28) Suh, J. S.; Huh, Y. M.; Jun, Y. W.; Song, H. T.; Kim, S.; Choi, J. S.; Lee, J. H.; Yoon, S.; Kim, K. S.; Shin, J. S.; Cheon, J. *J. Am. Chem. Soc.* **2005**, *127*, 12387.
- (29) Shin, J. S.; Lee, J. H.; Jun, Y. W.; Yeon, S. I.; Cheon, J. *Angew. Chem., Int. Ed.* **2006**, *45*, 8160.
- (30) Lee, J. H.; Jun, Y. W.; Yeon, S. I.; Shin, J. S.; Cheon, J. *Angew. Chem., Int. Ed.* **2006**, *45*, 8160.